GABA$_A$ Receptor α and γ Subunits Shape Synaptic Currents via Different Mechanisms*

Christine Dixon, Pankaj Sah, Joseph W. Lynch[1], and Angelo Keramidas[2]
From the Queensland Brain Institute, University of Queensland, Brisbane, Queensland, Australia 4072

Background: GABA$_A$R α2 and γ1 subunits are highly expressed in amygdala but their influence on synaptic currents is unknown.
Results: α2 subunits increased GABA affinity thereby slowing current deactivation; γ1 subunits reduced synaptic receptor clustering.
Conclusion: These subunits may differentially shape synaptic kinetics.
Significance: Understanding how α2 and γ1 subunits shape synaptic currents may help us understand amygdala processing mechanisms.

Synaptic GABA$_A$ receptors (GABA$_A$Rs) mediate most of the inhibitory neurotransmission in the brain. The majority of these receptors are comprised of α1, β2, and γ2 subunits. The amygdala, a structure involved in processing emotional stimuli, expresses α2 and γ1 subunits at high levels. The effect of these subunits on GABA$_A$R-mediated synaptic transmission is not known. Understanding the influence of these subunits on GABA$_A$R-mediated synaptic currents may help in identifying the roles and locations of amygdala synapses that contain these subunits. Here, we describe the biophysical and synaptic properties of pure populations of α1β2γ2, α2β2γ2, α1β2γ1 and α2β2γ1 GABA$_A$Rs. Their synaptic properties were examined in engineered synapses, whereas their kinetic properties were studied using rapid agonist application, and single channel recordings. All macropatch currents activated rapidly (<1 ms) and deactivated as a function of the α-subunit, with α2-containing GABA$_A$Rs consistently deactivating ~10-fold more slowly. Single channel analysis revealed that the slower current decay of α2-containing GABA$_A$Rs was due to longer burst durations at low GABA concentrations, corresponding to a ~4-fold higher affinity for GABA. Synaptic currents revealed a different pattern of activation and deactivation to that of macropatch data. The inclusion of α2 and γ1 subunits slowed both the activation and deactivation rates, suggesting that receptors containing these subunits cluster more diffusely at synapses. Switching the intracellular domains of the γ2 and γ1 subunits substantiated this inference. Because this region determines post-synaptic localization, we hypothesize that GABA$_A$Rs containing γ1 and γ2 use different mechanisms for synaptic clustering.

GABA$_A$ receptor (GABA$_A$R)[3] channels mediate the majority of inhibitory neurotransmissions in the mammalian brain.

These receptors are pentamers assembled from a large family of subunits, of which 19 members have so far been identified (1). Receptors targeted to the synaptic compartment are composed of two α, two β, and a single γ subunit, with the most highly expressed and best studied being the α1β2γ2 GABA$_A$Rs. However, GABA$_A$Rs that contain other subunits are also expressed in the brain (2).

The kinetics of inhibitory post-synaptic currents (IPSCs) at GABAergic synapses are determined by the biophysical properties of postsynaptic receptors (3, 4), and how they are clustered at the postsynaptic membrane (5, 6). The α subunit is a key determinant of the functional properties of GABA$_A$Rs (7, 8), and as such has a prominent role in setting the kinetics of IPSCs (3, 4, 9). The factors that regulate the synaptic clustering of GABA$_A$Rs are still being unraveled, but recent studies have shown that it involves complex, subunit-specific interactions with scaffolding proteins such as gephyrin (10–13), collybistin (14), and dystrophin (15).

The amygdala is a temporal lobe structure that plays a key role in processing fear, and amygdala dysfunction is associated with anxiety-related disorders such as generalized anxiety, depression, and post-traumatic stress. These disorders are commonly managed using benzodiazepines, which produce their therapeutic actions by enhancing the action of GABA at GABA$_A$Rs containing γ2 subunits (16, 17). However, as benzodiazepines act indiscriminately on GABA$_A$Rs expressed throughout the brain, their therapeutic activity is compromised by side effects such as sedation and tolerance.

Whereas the α1 and γ2 subunits are expressed throughout the central nervous system, the α2 and γ1 subunits have a restricted distribution, being prominent in brain structures such as the amygdala, forebrain, cerebellum, and hypothalamus (α2), and amygdala, pallidum, and substantia nigra (γ1) (2, 18, 19). The properties of receptors containing α1 and γ2 subunits, and their impact on synaptic currents have been extensively studied (4, 9, 20). In contrast, apart from limited information about their pharmacological profile (18, 19, 21), almost nothing

---

[3] The abbreviations used are: GABA$_A$R, γ-aminobutyric acid type A receptor; GABA, γ-aminobutyric acid; GAD65, glutamic acid decarboxylase isoform 65; GFP, green fluorescent protein; ID, intracellular domain; IPSC, inhibitory post-synaptic current; TM4, transmembrane domain 4; tcrit, critical value of t; ANOVA, analysis of variance.

is known about the impact of γ1-containing GABA$_A$Rs on inhibitory synaptic transmission.

Here we describe the kinetic and synaptic properties of GABA$_A$Rs containing α2 and γ1 subunits and compare them to those containing α1 and γ2 subunits. By providing new insights into the functional properties of α2- and γ1-containing GABA$_A$Rs, our study facilitates investigations into whether these GABA$_A$Rs contribute to synaptic currents in brain regions that mediate anxiety-related disorders such as fear, depression, and post-traumatic stress.

EXPERIMENTAL PROCEDURES

Cell Culture and Molecular Biology—Human α1 (pCIS2), α2 (pCIS2 or pcDNA3.1), β2 (pcDNA3.1+ or pcDNA3.1Zeo), γ1 (pcDNA3.1+), and γ2L (pcNDA3.1+) subunits were transfected in a subunit plasmid ratio of 1α:1β:3γ (total DNA was 0.2–2.0 μg), into HEK293 cells using Ca^{2+} phosphate-DNA coprecipitation. This transfection ratio ensured the incorporation of the γ subunit into the receptors. GABA$_A$Rs comprised only of α and β subunits were produced by transfecting these subunits at a plasmid ratio of 1:1. Cotransfecting the neuroligin splice variant neuroligin 2A (with HA tag), which was obtained from Addgene (USA) (22), facilitated the formation of heterosynapses. Enhanced GFP and CD4 were also transfected and acted as expression markers. Interchanging the intracellular domain (ID) and fourth transmembrane domain (TM4) domain of one γ subunit isoform with the other produced two γ subunit chimeras, which were transfected with α2 and β2 subunits. The two γ subunit chimeras were: 1) the γ2L-γ1, which expresses the γ2L subunit sequence from the N terminus up to the end of TM3 (up to Leu-317) and the ID and TM4 of the γ1 subunit sequence (from His-320), and 2) the γ1-γ2L, which contains the γ1 sequence from the N terminus to the end of TM3 (up to Leu-319) and the ID and TM4 of the γ2L sequence (from His-318). In a separate set of transfections we co-transfected the α2-containing GABA$_A$Rs along with rat gephyrin (with and without an N terminus GFP tag), and the human collybistin homologue, hPEM.

Primary neuronal cultures were prepared using standard protocols (23). The cortices of E18 rat embryos were triturated and plated at ~80,000 cells per 18-mm poly-D-lysine-coated coverslip in DMEM with 10% fetal bovine serum. After 24 h the entire medium was replaced with Neurobasal medium including 2% B27 and 1% GlutaMAX supplements; a second feed after 1 week replaced half of this medium. Neurons were grown for 3 to 5 weeks *in vitro* and the heterosynapse co-cultures were prepared by directly introducing transfected HEK293 cells onto the primary neuronal cultures. Recordings of synaptic currents were done 1–3 days later.

Immunofluorescent Labeling—Coverslips with cells were fixed for 5–10 min in 4% paraformaldehyde in phosphate-buffered saline, then blocked and permeabilized in 3% bovine serum albumin with saponin (0.05%) for 30 min. HA-tagged neuroligin 2A was labeled with rabbit anti-HA (Santa Cruz, 1/100) and GABAergic terminals were labeled for the GABA synthesizing enzyme GAD65 (mouse anti-GAD65, Chemicon/Millipore, 1/10,000). Primary antibodies were added to blocking solution overnight at room temperature, the cells were washed and sec-

ondary antibodies were applied at 1/500 for 30 min. Coverslips were mounted using DAKO fluorescent mounting medium and imaged on upright fluorescent and confocal microscopes.

Electrophysiology—All experiments were performed at room temperature in either the whole cell or outside-out patch configuration of the patch clamp technique, at a holding potential of −70 mV. The intracellular solution was composed of (in mM): 145 CsCl, 2 CaCl$_2$, 2 MgCl$_2$, 10 HEPES, and 10 EGTA, adjusted to pH 7.4 with CsOH. Cells and patches were continuously perfused with extracellular solution made up of (in mM): 140 NaCl, 5 KCl, 2 CaCl$_2$, 1 MgCl$_2$, 10 HEPES, and 10 D-glucose, adjusted to pH 7.4 with NaOH. The liquid junction potential between the intra- and extracellular solutions was calculated to be 4.0 mV (24). A double-barreled glass tube was mounted onto a piezo-electric translator (Siskiyou) to achieve rapid solution exchange (<1 ms) over outside-out patches by lateral movement of the glass tube. Synaptic currents were filtered (−3 dB, 4-pole Bessel) at 4 kHz and sampled at 10 kHz, whereas the macropatch recordings were filtered at 10 kHz and sampled at 30 kHz. Synaptic and macropatch data were recorded using a Multiclamp 700B amplifier and pClamp 9 software. Single channel currents were recorded using an Axopatch 200B amplifier, pClamp 10 software, filtered at 10 kHz and sampled at 50 kHz. Current traces were filtered off-line at 5 kHz for making figures.

Stock solutions of flunitrazepam and diazepam were kept frozen and diluted to the desired concentration in extracellular solution on the day of recording. Typically, at least 3 min of spontaneous activity was recorded before and during drug application. To preserve network activity for spontaneous recordings, the drug solution was targeted to the recorded cell, whereas the extracellular solution was washed over the surrounding area. Drug washout was obtained in about half of the cells recorded, and was averaged with the baseline data to minimize time-dependent effects.

Analysis—Data are presented as mean ± S.E. Exponential equations were fit to the rising phase (10–90%) and current decay (weighted double- or mono-exponentials) of macropatch and synaptic currents as previously described (7) using Axograph X. Each current from a recorded cell or patch was analyzed separately and then averaged for that record. These averages were then pooled into data sets, from which means were calculated. Currents containing double events or artifacts in current rise and decay were manually excluded. Current-voltage (*I-V*) experiments were done by measuring single channel current amplitude at the corresponding voltage, for voltages of (in mV): ±70, ±35, ±15, and 0. The current reversal potential was read directly from the *I-V* plots.

Single channel kinetic analysis was done using QuB software. Current records were idealized at a cut-off resolution of 70 μs. The idealized records were then divided into discrete, single channel active periods by applying a tcrit shut duration. Tcrit values were determined for each patch and selected so as to retain the three briefest shut components (common to all records) in the dwell distributions as previously outlined (7, 25). Clusters (3 mM GABA) and bursts (2 μM GABA) of activity were accepted for deriving an activation mechanism if they contained >10 or 3 events, respectively (for estimating the mean

burst duration at 2 μM GABA, bursts that contained $\geq$2 events were also included). This resulted in open dwell distributions that were also composed of three components, when fitted using the "star" function in QuB. Three shut and three open components were taken to represent the minimum number of corresponding states for constructing activation schemes. Mechanisms were then postulated and used to generate fits to the dwell distributions by maximum likelihood fitting (26, 27). The procedure optimized the rate constants and produced a goodness of fit value (log likelihood) that was used to evaluate the schemes. Data obtained at 3 mM GABA were first analyzed for determining the best consensus scheme for all four GABA$_A$Rs. The rate constants thus obtained were averaged across records for each GABA$_A$R. To estimate the rate constants for the binding (k_{+1}) and unbinding (k_{-1}) of GABA, the averaged rate constants for activation at 3 mM GABA were fixed. Binding steps were then appended to the first shut state in the scheme(s) (A_2R^1), and the scheme was re-fitted to data sets that included low (2 μM) data, allowing k_{+1} and k_{-1} to vary freely in the fitting. Combining several records at 2 μM GABA was required to increase the number of total events for that concentration. These were then combined with data obtained at 3 mM GABA to produce a data set for simultaneous fitting to the mechanism. The binding affinity ($K_d = k_{-1}/k_{+1}$) was then calculated for each data set and averaged for each GABA$_A$R. Macropatch simulations were generated by the finalized mechanism (with all rate constants). The "dose-response" function in QuB was used to simulate macropatch currents, after setting the number of channels to 1000 and the K_d values of α1- and α2-containing GABA$_A$Rs to 25 and 100 μM, respectively. Exponential fitting to the rise and decay phases of the simulated currents was done in QuB or pClamp 10 (Clampfit).

RESULTS

Incorporation of the γ-Subunit into GABA$_A$Rs—On the basis of conductance and kinetic properties, GABA$_A$Rs comprising of α, β, and γ subunits are clearly distinguishable on the single channel level from those composed of α and β subunits. $\alpha\beta\gamma$ receptors activate with a predominant unitary conductance of $\sim$26 pS (at -70 mV) and exhibit complex bursting behavior with relatively long burst durations. In contrast, $\alpha\beta$ receptors under similar recording conditions have a conductance of $\sim$15 pS and exhibit simple, relatively short periods of activity (28, 29). We wished to investigate the presence of GABA$_A$Rs comprised only of α and β subunits in our standard $\alpha\beta\gamma$ receptor transfections to determine whether our transfections produced pure populations of $\alpha\beta\gamma$ receptors. To facilitate the identification of $\alpha\beta$ receptors we transfected α1 with β2 or α2 with β2 at an α:β plasmid ratio of 1:1, and recorded the resulting single channel activity. $\alpha\beta$ receptors comprised of α1 and β2 subunits opened to 1.0 pA (γ = 12.7 pS, n = 7 pooled), whereas α2β2 receptors opened to a mean amplitude of 1.1 pA (γ = 14.0 pS, n = 8 pooled). No activations were observed that exceeded these levels (Fig. 1*A*). We then looked for these $\alpha\beta$ receptor activations in patches excised from cells transfected with an α:β:γ plasmid ratio of 1:1:3. To obtain an estimate of the incidence of $\alpha\beta$ ($\sim$1 pA) *versus* $\alpha\beta\gamma$ ($\sim$2 pA) receptor activity we conducted a count of discrete (well separated) single channel
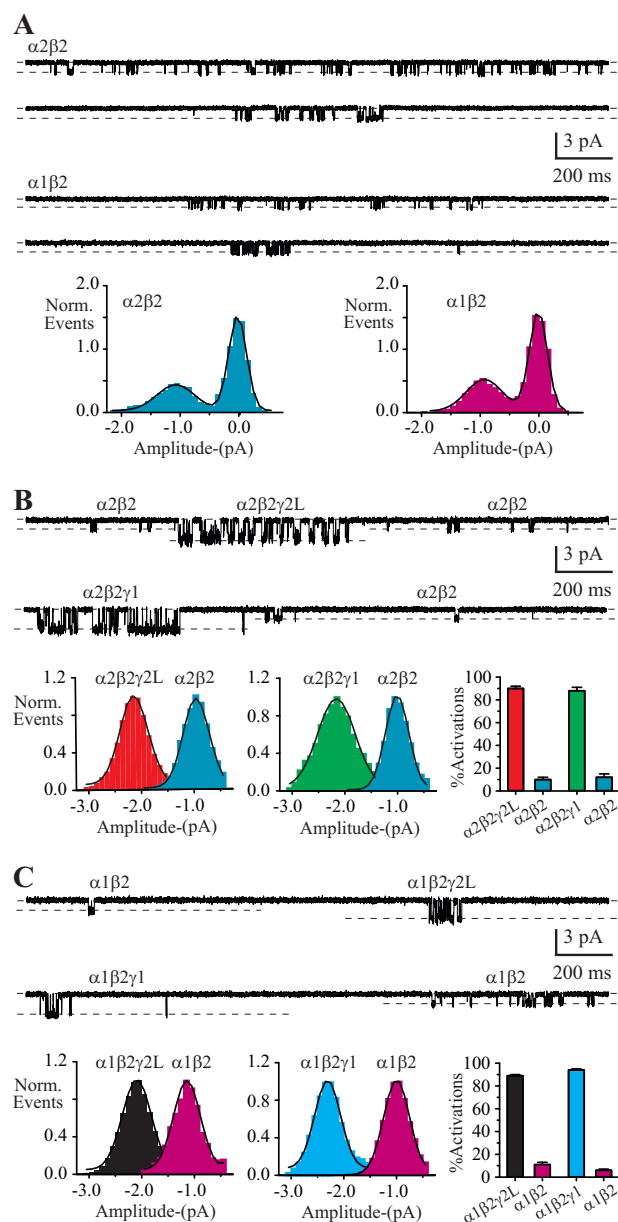
FIGURE 1. **Distinguishing $\alpha\beta$ and $\alpha\beta\gamma$ receptors.** *A*, sample single channel recordings from patches expressing α2β2 (*above*) and α1β2 (*below*) receptors, along with the corresponding amplitude histograms. Transfecting only α and β subunits produced GABA-activated channel activity of $\sim$1 pA in amplitude. *B* and *C*, recordings from patches excised from cells transfected with α2, β2, γ2L or γ1 (*B*), or α1, β2, γ2L or γ1 (*C*), showing examples of $\alpha\beta\gamma$ ($\sim$2 pA) and $\alpha\beta$ ($\sim$1 pA) channel activations in the same patches. The accompanying amplitude histograms show that $\alpha\beta$ and $\alpha\beta\gamma$ channels are clearly distinguishable in terms of amplitude, and the *bar graphs* on the far right show the relative proportions of $\alpha\beta\gamma$ and $\alpha\beta$ channel activations, averaged over 3–5 patches, for each $\alpha\beta\gamma$ channel transfection type.

activations mediated by both receptor types. Activations (burst or clusters) that were due to a single receptor were determined as outlined under "Experimental Procedures." Counting the relative numbers of well separated periods of activity minimized the false positive detection of $\alpha\beta$ receptor activity, as it is well known that $\alpha\beta\gamma$ channels can transition to sublevels within activations (7). The appearance of $\alpha\beta$ channel activations in all four $\alpha\beta\gamma$ receptor transfections was minimal. Transfections that included α2, β2, and γ2L subunits exhibited α2β2
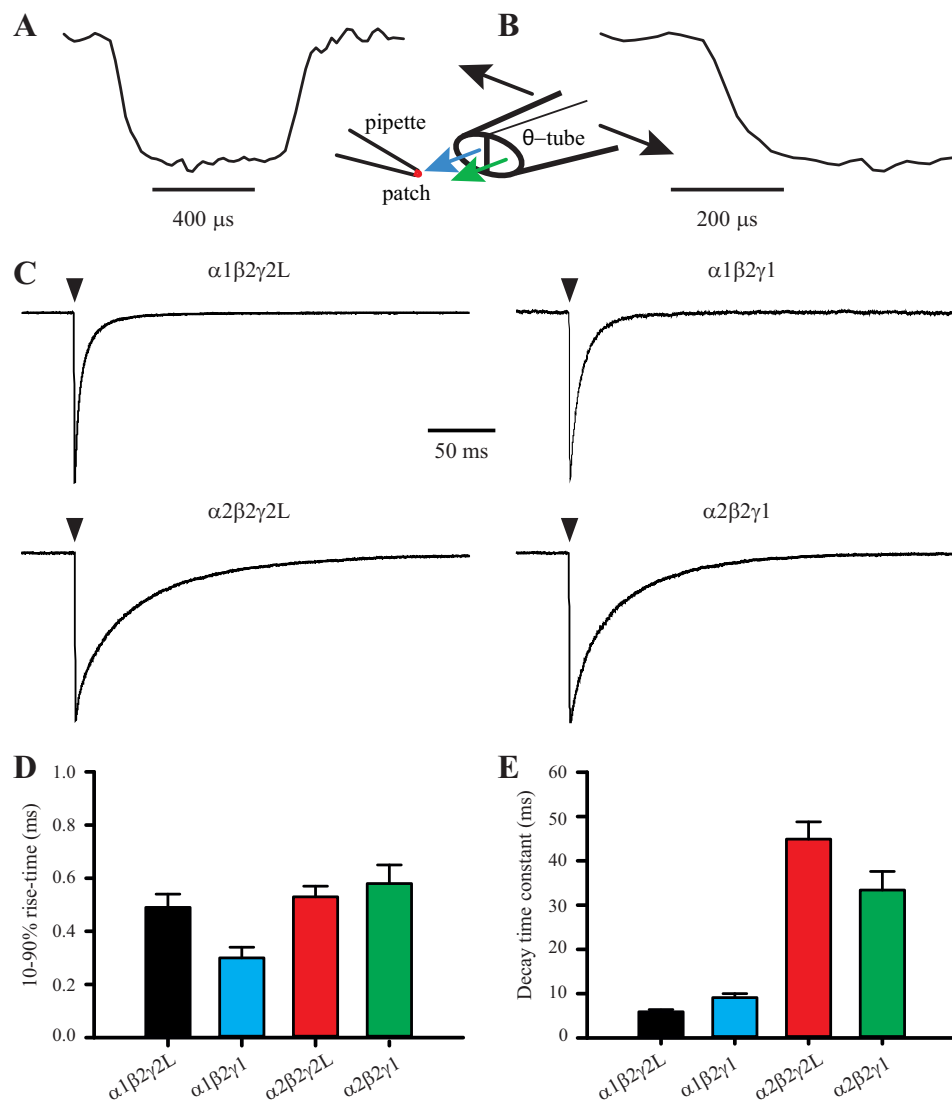
FIGURE 2. **Macropatch recordings.** *A* and *B,* open pipette response (downward deflection) elicited by rapid, lateral translation of a double-barrel glass tube (*θ-tube, inset*). One of the barrels contained a standard extracellular solution, whereas the other contained a barrel diluted by 50% with distilled water. Open pipette responses were used to optimize agonist application onto macropatches. *C,* averaged sweeps of macropatch currents recorded from patches express-ing, α1β2γ2L, α1β2γ1, α2β2γ2L, and α2β2γ1 GABA$_A$Rs in response to ~1 ms application of 3 mM GABA (*arrowhead*). The currents for all four GABA$_A$Rs develop rapidly, with a 10–90% rise times of <1 ms. Current deactivation has a slower time course and shows a clear α-subunit isoform correlation, with α1-containing receptors deactivating more rapidly than those containing the α2 subunit. Averaged data for the 10–90% rise time (*D*) and deactivation rate (*E*) for the macropatch data.

receptor activations that constituted 10 ± 2% (*n* = 3) of the total activity, whereas those that included α2, β2, and γ1 sub-units produced α2β2 receptor activations that were only 12 ± 3% (*n* = 5) of the total activity (Fig. 1*B*). In patches expressing α1, β2, and γ2L subunits the incidence of α1β2 receptor-me-diated activity was 11 ± 2% (*n* = 4) of the total measured. Similarly, when expressing α1, β2, and γ1 subunits, 6 ± 1% (*n* = 3) of the activations were of the α1β2 phenotype (Fig. 1*C*). Hence, our standard transfection ratio produced mainly signa-ture αβγ channel activations, ranging from 88 to 94% of the total number. This result is consistent with a study that deduced that αβγ receptors are the almost exclusively pre-ferred assembly, even with a transfection ratio of 1:1:1 (28).

Rapid GABA Application onto Macropatches—To under-stand the impact of γ (γ1 and γ2L) and α (α1 and α2) subunits on the intrinsic properties of GABA$_A$Rs we recorded ensemble

currents from outside-out patches excised from HEK293 cells expressing α1β2γ2L, α1β2γ1, α2β2γ1, or α2β2γ2L GABA$_A$Rs in response to brief (<1 ms, Fig. 2, *A* and *B*) saturating GABA (3 mM). Receptors containing α1 subunits activated relatively rap-idly as compared with those containing α2 subunits. α1β2γ2L and α1β2γ1 GABA$_A$Rs activated with 10–90% rise times of 0.49 ± 0.05 ms (*n* = 10) and 0.30 ± 0.04 ms (*n* = 6, Fig. 2, *C* and *D*), respectively, whereas, α2β2γ2L and α2β2γ1 GABA$_A$Rs activated with rise times of 0.53 ± 0.10 ms (*n* = 7) and 0.58 ± 0.07 ms (*n* = 9, Fig. 2, *C* and *D*), respectively. A two-way ANOVA revealed a correlation between rise time and the α subunit (*p* = 0.02), but not the γ subunit isoform. The deacti-vation phase of the currents was also substantially slower for GABA$_A$Rs containing the α2 subunit (Fig. 2, *C* and *E*). The weighted deactivation time constants for α1β2γ2L and α1β2γ1 GABA$_A$Rs were 5.9 ± 0.5 (*n* = 10) and 9.1 ± 0.9 ms (*n* = 6),
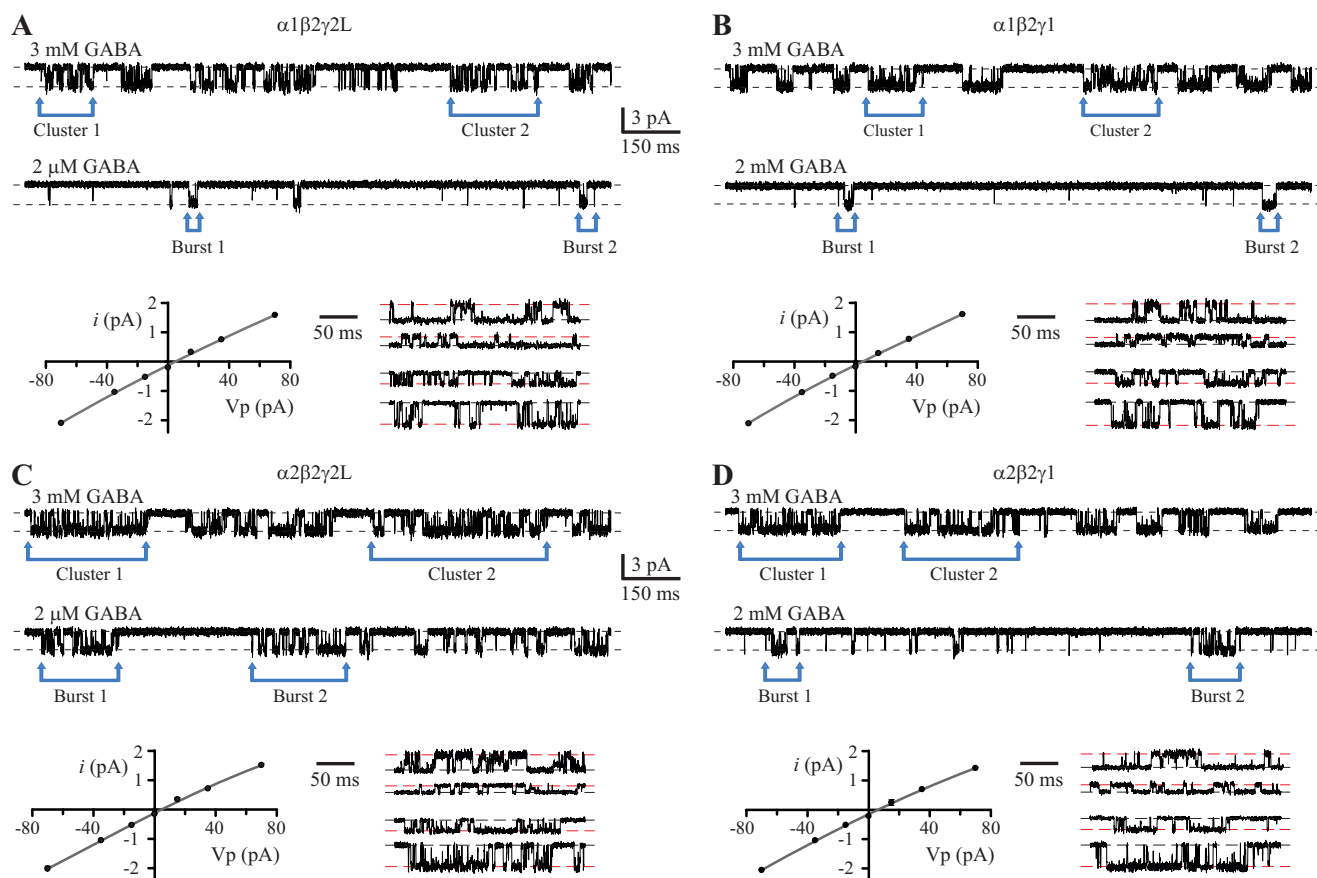
FIGURE 3. **Single channel activations and I-V.** Single channel currents elicited by saturating (3 mM, *above*) and subsaturating (2 μM, *below*) concentrations of GABA for patches expressing (A) α1β2γ2L, (B) α1β2γ1, (C) α2β2γ2L, and (D) α2β2γ1 GABA_ARs. The tcrit values at 3 mM GABA, ranged between 25 and 35 ms, whereas those for activity elicited by 2 μM GABA ranged between 35 and 45 ms. Accompanying the activations are the *I*-V relationships of each receptor, generated from averaged data from 3 to 5 patches, along with sample currents at ±70 and ±35 mV (the open level is indicated by a *red broken line*). The main subunit-dependent differences are the duration of discrete active periods, especially at 2 μM GABA. Bursts of activity from α2-containing receptors remain active for 3–4-fold longer than bursts recorded from α1-containing receptors. The burst lengths for the four GABA_ARs follow the same pattern as the deactivation rates of macropatch currents.

respectively. The presence of the α2 subunit dramatically slowed current decay with the mean decay time constant of α2β2γ2L GABA_ARs, being 44.9 ± 3.9 ms ($n = 7$), and that of α2β2γ1 GABA_AR-mediated currents being 33.4 ± 4.2 ms ($n = 9$). Again, a two-way ANOVA revealed a highly significant correlation between the α subunit and current decay ($p < 0.0001$), but not the γ subunit isoform. These results confirm previous results showing that α1β2γ2 GABA_ARs (30, 31) display significantly faster activation and deactivation kinetics, as compared with those containing α2 subunits (8, 32). Thus, whereas the α subunit isoform has a profound affect on ensemble current kinetics, mainly by slowing current deactivation, replacing γ2L subunits with γ1 has no effect on the kinetics of expressed receptors.

Single Channels Analysis and Activation Mechanisms—We next asked how the α2 subunit enables the current to persist as the GABA concentration drops to zero. Single channel currents were recorded at saturating (3 mM) and low (2 μM) concentrations of GABA, which mimic the concentration profile at the onset and near the end of a synaptic event, respectively. The initial analysis focused on the durations of discrete activations (bursts and clusters of bursts) that define the activity of a single ion channel, the open state occupancy within activations (P_o)

and current voltage (*I*-V) relationships. All four GABA_ARs exhibited single channel currents that were ∼2 pA in amplitude at −70 mV and had *I*-V with mild inward rectification (Fig. 3). Single channel conductance were calculated at −70 mV after correcting the driving force for reversal (4.5–5.0 mV) and liquid junction (4.0 mV) potentials. The calculations yielded conductance values of 26.6 (α1β2γ2L), 26.9 (α1β2γ1), 25.7 (α2β2γ2L), and 26.7 pS (α2β2γ1). All receptors showed at least 2 gating modes, which were equally prevalent among the receptors. This phenomenon has been observed in other GABA_ARs (25, 30), but as we were ultimately interested in determining the factors that slowed the deactivation phase of α2-containing receptors, the different modes of activity for each GABA_AR were pooled for further analysis. Table 1 summarizes the durations of the activations and the P_o values for the four channel types. At 3 mM GABA, the mean durations of clusters of activity ranged between 148 and 206 ms, with a small, but non-significant trend toward longer activations for GABA_ARs harboring the α2 subunit. The same rank order of, α1β2γ2L < α1β2γ1 < α2β2γ1 < α2β2γ2L was observed for mean burst durations elicited by 2 μM GABA, but the differences here were more dramatic. Burst durations for α1-containing GABA_ARs ranged between 23 and 27 ms (Fig. 3, *A* and *B*). This was ∼3–4-fold briefer than those

TABLE 1

Single channel current parameters

Single channel activation parameters of GABA$_A$ receptor isoforms

	Intraburst P$_o$		Mean burst length	
Channel	3 mM GABA	2 μM GABA	3 mM GABA	2 μM GABA[a]
			ms	
α1β2γ2L	0.56 ± 0.04	0.37 ± 0.01	148 ± 16	23 ± 2
α1β2γ1	0.58 ± 0.03	0.44 ± 0.03	167 ± 17	27 ± 3
α2β2γ2L	0.61 ± 0.04	0.58 ± 0.01	206 ± 7	99 ± 13
α2β2γ1	0.66 ± 0.03	0.55 ± 0.02	187 ± 15	56 ± 7

[a] Estimates from data that include bursts with ≥2 events. Data represent averages from 3 to 8 patches.

for α2β2γ2L receptors that activated for a mean duration of 99 ms (Fig. 3*C*), whereas bursts of activity mediated by α2β2γ1 receptors were of intermediate durations, being 56 ms (Fig. 3*D*, Table 1). The time spent in conducting configurations was similar for all four receptors, especially at 3 mM GABA, yielding P$_o$ values of ~0.6–0.7. At 2 μM GABA, the P$_o$ values mirrored the rank order of burst durations, but the absolute differences were smaller. It is notable, however, that the P$_o$ value for the α2β2γ1 and α2β2γ2L receptors at 2 μM GABA were indistinguishable from those of α1β2γ2L and α1β2γ1 receptors at 3 mM GABA, suggesting that α2-containing GABA$_A$Rs dwell in conducting states for longer intervals. Overall, the most noteworthy difference between the receptor types was the mean duration of bursts elicited by 2 μM GABA. This likely underlies the longer deactivation times for receptors harboring the α2 subunit. In support of this inference, synaptic currents mediated by other ligand-gated ion channels have also been shown to deactivate as a function of the durations of single channel bursts of activity (33–35).

We then proceeded to analyze the open and shut dwell time distributions for the purpose of deriving a consensus mechanism for channel activation. A mechanism that accounted for the salient properties of agonist affinity and gating kinetics would allow us to determine the underlying kinetic factors that give rise to the differential ensemble and single channel currents between the four GABA$_A$Rs, within the same quantitative framework. This would facilitate a direct comparison between receptors. We commenced this analysis by plotting shut dwell histograms to activations elicited by 3 mM and 2 μM GABA. These histograms were then fitted to mixtures of exponentials to determine the minimum number of individual components that were apparent across patches and at both concentrations of GABA, and the tcrit values required to preserve them. Clusters and bursts of activity divided by this method yielded shut and open dwell histograms with three components each, as shown in Fig. 4*A*. This was consistent across all four receptor types suggesting that, in kinetic terms, they were all broadly similar.

We first considered clusters of activity at saturating (3 mM) GABA because this ensures binding site saturation, allowing us to omit the binding steps in the initial analysis. The number of components in the shut and open histograms was taken to represent the minimum number of functional states in the underlying activation mechanism. Mechanisms with three shut and open states were connected in various schemes and used to fit the dwell histograms to mixtures of exponentials by maximum likelihood fitting (26, 27). The fitting method uses the (apparent) open and shut dwell distributions to compute the likeli-

hood that the data are represented by a postulated sequence of open and shut times. The free parameters to be fitted, for each postulated mechanism, are the rate constants governing the transitions between states, which are optimized to maximize the probability of observing the data. Mechanisms that best described the activity included schemes that were linear with some branching and schemes containing looped connections (Fig. 4, *B* and *D*). The schemes were then evaluated and ranked on the basis of a goodness of fit measure (log likelihood) and how accurately the schemes recapitulated the time constants and fractions of the initial "star" fit of the data. The three linear-branched schemes (Fig. 4, *B* and *D*, Schemes 1–3) that generated the best fits to the data and the single best, looped scheme (Scheme 4 as shown in Fig. 4). Similar linear-branched schemes have previously been reported for GABA$_A$R activation (7, 25, 36). Scheme 3 has previously been reported as an activation mechanism for α1β2γ2S and α3β3γ2S GABA$_A$Rs (7). This scheme also fit the activity for γ2L-containing GABA$_A$Rs. However, we found that Scheme 1 produced higher log likelihood values for γ1-containing channels and was competitive with Scheme 3 for γ2L-containing channels. Summing the likelihood (ΣLL) values for each scheme over all four GABA$_A$Rs revealed Scheme 1 as the best overall arrangement. Schemes that contained loops did not generally fit the data as well as linear-branched schemes, but Scheme 4 (Fig. 4*D*) adequately described most of the data, even though it was not as competitive as Schemes 1–3. On the basis of the ΣLL and most accurate reproduction of individual components, in terms of time constants and fractions of the dwell distribution, Scheme 1 was chosen as the consensus mechanism for further analysis of rate constants for GABA activation. Rate constants were computed for each patch, averaged for each receptor subtype (Table 2), and the equilibrium constant for each state transition was determined (Table 3). Equilibrium constants were broadly similar across receptor types. One consistent difference was the constant between the first and second shut states, A_2R^1 and A_2R^2 (Φ). GABA$_A$Rs expressing the γ2 subunit had Φ constants that were >1, whereas those for γ1-containing receptors were <1. Φ was subunit specific, suggesting that the γ subunit is not only involved in the activation process, but its contribution to activation is γ isoform dependent. The mean lifetime of A_2R^{2*} was also prolonged by the presence of the α2 subunit, consistent with the higher P$_o$ values for these channels. However, none of the equilibrium constants differed to an extent that would adequately account for the longer burst durations for α2-containing receptors at 2 μM GABA.

Bursts of activity at 2 μM GABA were used to estimate the rate constants for GABA binding. Sequential, identical binding steps were appended to A_2R^1 (*red arrows* in Fig. 4) and fitted to dwell time histograms derived from data obtained at high and low GABA, which constituted a single data set. The rate constants for the transitions downstream of the binding steps were fixed to the mean values obtained at 3 mM GABA for each receptor subtype (Table 2), allowing only the GABA association and dissociation rate constants to vary during the fitting. More consistent binding rate constants were obtained when data from multiple patches exposed to 2 μM GABA were combined. Three or more data sets were used for each GABA$_A$R, and mean
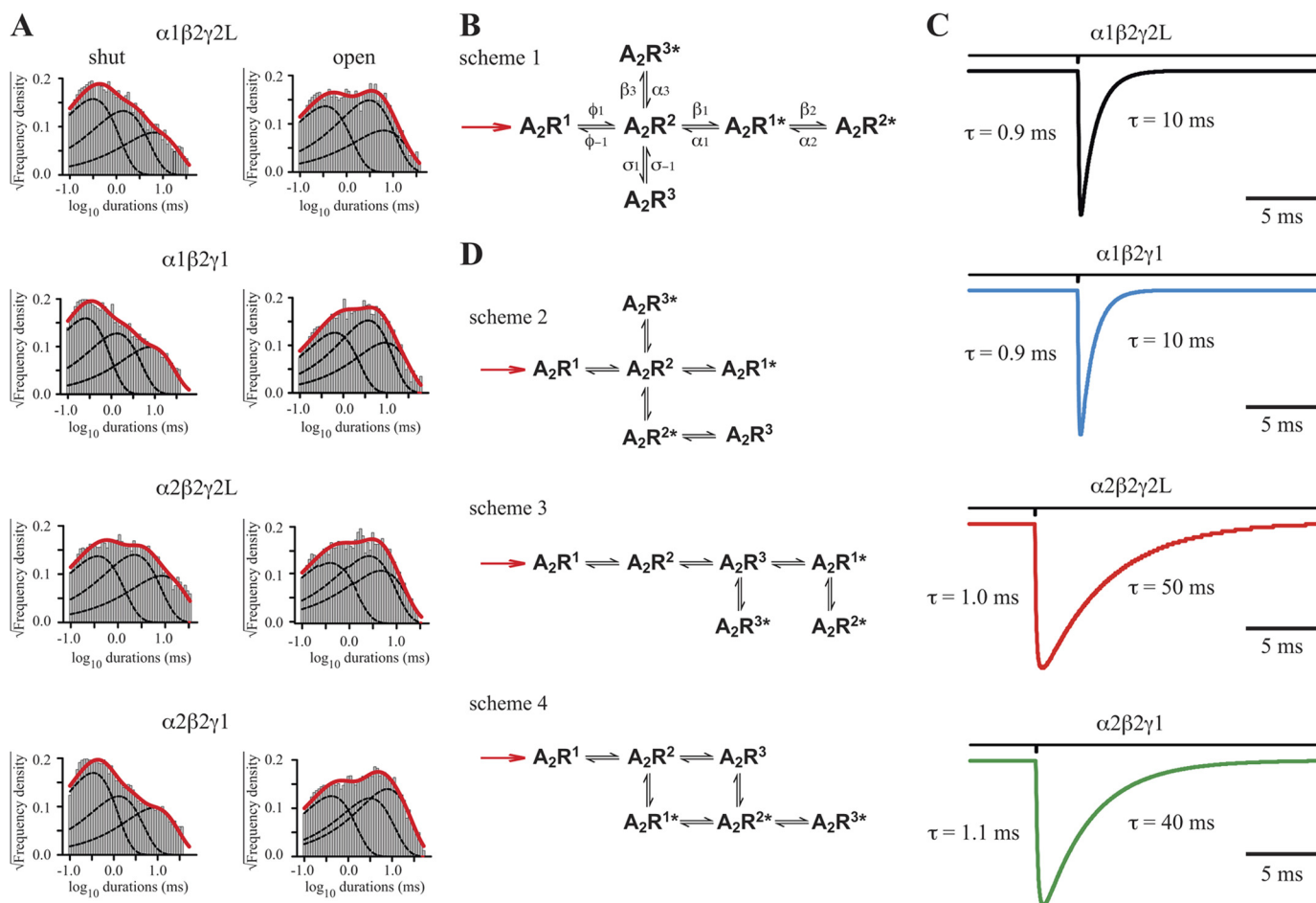
FIGURE 4. **GABA-gated activation mechanisms.** *A*, shut and open dwell histograms for data obtained at 3 mM GABA. The histograms shown for all four receptors have three shut and three open components, suggesting that they are kinetically similar. *B*, consensus activation mechanism for activation by GABA that described the single channel activity (histograms) most accurately for the four receptors. *A* denotes the agonist and *A$_2$* denotes a doubly liganded receptor, *R*. The *superscript numbers* denote the state number and the *asterisk* denotes open, conducting states. The *letters above* the *double arrows* that connect states are the rate constants governing the forward and backward transitions. *C*, simulated ensemble currents for α1β2γ2L, α1β2γ1, α2β2γ2L, and α2β2γ1 GABA$_A$Rs using Scheme 1 with averaged rate constants (Table 2). The macropatch currents were generated by setting the channel number to 1000 and the agonist application time to 1 ms in QuB. The time constants for activation and deactivation are shown for each current. *D*, other postulated schemes that fit the data adequately, including Scheme 2 (3) and a scheme containing looped connections (Scheme 4). Note that all schemes have at least one shut-shut transition between the binding steps (*red arrows*) and the open states.

TABLE 2

Rate constants for Scheme 1 (Fig. 4B)

Rate constants determined for data at 3 mM GABA. Means are calculated from 3 to 4 data sets per receptor.

	$\varphi 1$	$\varphi -1$	$\sigma 1$	$\sigma -1$	$\beta 1$	$\alpha 1$	$\beta 2$	$\alpha 2$	$\beta 3$	$\alpha 3$
α1β2γ1	830 ± 68	1254 ±161	181 ±32	511 ±68	2210 ±280	1388 ±208	143 ±322	750 ±90	849 ±159	638 ±346
α1β2γ2L	1039 ±187	800 ±76	323 ±46	621 ±29	1018 ±180	1860 ±171	263 ±178	620 ±61	960 ±160	882 ±42
α2β2γ1	684 ±210	912 ±219	240 ±56	327 ±139	1405 ±265	882 ±348	482 ±414	337 ±196	735 ±220	1634 ±752
α2β2γ2L	1490 ±292	1420 ±254	325 ±88	360 ±95	1547 ±239	1536 ±374	1224 ±521	345 ±76	809 ±229	1231 ±571

TABLE 3

Equilibrium constants for Scheme 1 (Fig. 4B)

	Φ $(\varphi 1/\varphi -1)$	Σ $(\sigma 1/\sigma -1)$	E1 $(\beta 1/\alpha 1)$	E2 $(\beta 2/\alpha 2)$	E3 $(\beta 3/\alpha 3)$	K_d (k_{-1}/k_{+1})
α1β2γ1	0.67	0.35	1.60	0.20	1.33	100 ± 12
α1β2γ2L	1.30	0.52	0.55	0.42	1.10	99 ± 17
α2β2γ1	0.75	0.73	1.60	1.37	0.45	25 ± 4
α2β2γ2L	1.05	0.90	1.01	3.55	0.66	28 ± 6

values for GABA binding affinity (K_d) were obtained (Table 3). This analysis revealed clear differences in affinity that closely correlated with the α subunit isoform, but not the γ isoform, and is consistent with the lack of involvement of γ subunits in GABA binding. For α1-containing receptors the GABA associ-

ation rate constants (k_{+1}) varied between 2.2 × 10^6 and 3.6 × 10^6 M^{-1} s^{-1} and the dissociation rate constant (k_{-1}) varied between 350 and 450 s^{-1}, yielding a mean K_d of ~100 μM for both receptors. In contrast, α2-containing receptors had a 3–4-fold greater affinity for GABA. The k_{+1} values estimated for these two GABA$_A$Rs ranged between 4.0 and 4.5 × 10^6 M^{-1} s^{-1}, whereas the k_{-1} values varied between 75 and 130 s^{-1}, producing mean K_d values of ~25–30 μM for GABA.

As an independent (and non-equilibrium) test for Scheme 1 as a suitable consensus mechanism for activation of multiple types of GABA$_A$Rs, we used this scheme with the respective mean rate constants for gating for the four channels, and K_d

values of 100 and 25 μM for α1- and α2-containing GABA$_A$Rs, respectively, to generate simulated macropatch ensemble currents (Fig. 4C). The simulated ensemble currents all activated rapidly ($\sim$1 ms), being only marginally slower than the measured macropatch currents (Fig. 2). For α1-containing GABA$_A$Rs the simulated ensemble currents were similar, but not identical. The deactivation phase of these currents, fitted to two exponential equations, produced single weighted time constants of $\sim$10 ms, which was also close to the measured values of $\sim$6–9 ms. Similarly, Scheme 1 produced simulated ensemble currents that activated with 10–90% rise times of $\sim$1 ms for both α2-containing receptors and deactivation time constants of $\sim$40 ms for α2β2γ1 GABA$_A$Rs (measured $\sim$33 ms) and $\sim$50 ms for α2β2γ2L GABA$_A$Rs (measured $\sim$45 ms). These estimates corresponded closely with the measurements from experimental currents (Fig. 2), again validating Scheme 1 as an accurate general descriptor of both single channel activations and macropatch currents for the four synaptic GABA$_A$Rs considered here.

Synaptic Currents Mediated by α1β2γ2L, α1β2γ1, α2β2γ1, and α2β2γ2L GABA$_A$Rs—We have shown that α1β2γ2L, α1β2γ1, α2β2γ1, and α2β2γ2L GABA$_A$Rs can be described by a single kinetic mechanism with the key difference being that receptors containing α2 subunits have a significantly higher affinity for GABA, resulting in slower current deactivation times. In contrast, the γ subunit has little or no impact on the kinetics of ensemble currents. We therefore predicted that the kinetics of synaptic currents mediated by these receptors would be dominated by the α subunit. This prediction was tested in engineered heterosynapses formed between HEK293 cells and cultured cortical neurons, enabling us to examine the properties of synaptic currents mediated by populations of GABA$_A$Rs of defined subunit composition. Importantly, synaptic currents at these engineered synapses should not be affected by errors due to voltage clamp or electronic distortions commonly present when recording synaptic currents from neurons. Mature cortical neurons readily formed GABAergic synaptic contacts on HEK293 cells transfected with the desired GABA$_A$R. The synapses were observable as GAD65-positive contacts on the surface of the HEK293 cells (Fig. 5A). Higher resolution confocal images of cells where neuroligin 2A had been labeled to represent the postsynaptic density showed a close correspondence between neuroligin 2A and GAD-65 positive synaptic contacts confirming assembly of GABAergic synapses on HEK293 cells (Fig. 5B).

Whole cell recordings from transfected HEK293 cells in co-culture with cortical neurons exhibited spontaneous synaptic currents of variable amplitude that ranged between $\sim$20 and 200 pA for all four receptor types (Fig. 5C). IPSCs mediated by the well characterized α1β2γ2L GABA$_A$Rs activated rapidly, with mean 10–90% rise times of 1.2 $\pm$ 0.2 ms and decayed with a mean time constant of 4.0 $\pm$ 0.8 ms ($n = 3$ cells). These values are similar to rise time and offset time constants for the same receptors expressed in macropatches (Fig. 2). Moreover, they are similar to previously reported recordings of synaptic currents at synapses expressing α1β2γ2 GABA$_A$Rs (4, 9), including studies on neuronal types that are not susceptible the distorting effects of cable filtering (20). Together, these results show that
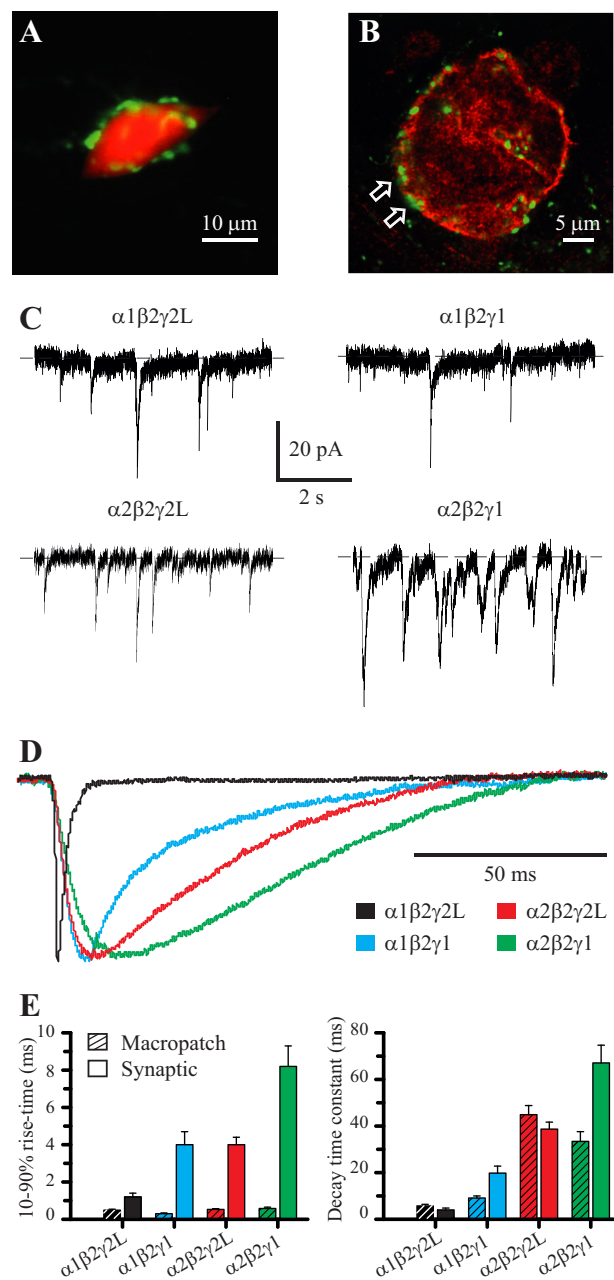
FIGURE 5. **Heterosynapses expressing GABA$_A$Rs.** *A*, fluorescent micrograph of an HEK293 cell expressing red fluorescent protein and neuronal GAD65-positive contacts (*green*) being formed on the HEK293 cell. *B*, confocal section of an HEK293 cell showing HA-tagged neuroligin (*red*) and neuronal GAD65-positive contacts (*green, arrows*). *C*, segments of whole cell recordings from HEK293 cells transfected with the indicated GABA$_A$Rs, in co-culture with cortical neurons. Synaptic currents were of variable amplitude and frequency from cell to cell, but were consistently recorded across transfections. *D*, averaged synaptic currents for the four GABA$_A$Rs as indicated. The inclusion of the α2 and γ1 subunits effectively reduced the rates of current activation and deactivation. *E*, pooled data for the activation (*left*) and deactivation (*right*) rates for macropatch and synaptic currents.

synapses that form in co-cultures faithfully recapitulate functional synapses.

As compared with those mediated by α1β2γ2L receptors, synaptic currents mediated by the other three GABA$_A$Rs showed markedly different activation and deactivation profiles (Fig. 5, *D* and *E*). The rise times for these synaptic currents were all slower than their respective activation rates in macro-

patches. α1β2γ1 and α2β2γ2L receptor synaptic currents had mean 10–90% rise times of 4.0 ± 0.7 ($n = 4$) and 4.0 ± 0.5 ms ($n = 7$), respectively. The rise time of the α2β2γ1 receptor-mediated currents was exceptionally slow, being 8.2 ± 1.1 ms ($n = 5$). A two-way ANOVA revealed that both α and γ subunit isoforms had a significant effect on current activation ($p <$ 0.001). Similarly, as compared with macropatches, the deactivation of IPSCs mediated by α1β2γ1 and α2β2γ1 GABA$_A$Rs were substantially slower (Fig. 4*E*), with mean time constants of 19.8 ± 3.0 ($n = 4$) and 67.1 ± 7.6 ms ($n = 7$), respectively. The α2β2γ2L GABA$_A$R generated IPSCs that deactivated with an intermediate time constant (38.7 ± 3.0 ms, $n = 7$). Here too, a two-way ANOVA test indicated that both α and γ subunit isoforms had a significant effect on current deactivation ($p <$ 0.001). Synaptic currents mediated by α2-containing receptors had the slowest decay time constants, but this could only partially be explained by the macropatch and single channel data. These data suggest that α2 and γ2L subunits play distinct roles in determining the kinetics of GABA$_A$R-mediated IPSCs. Receptors incorporating the α2 subunit mediate currents with slower activation and deactivation kinetics, whereas the presence of the γ2L subunit tended to accelerate both activation and deactivation. The antagonistic effect between α2 and γ2L is best illustrated in α2β2γ2L GABA$_A$Rs, whose currents activated more slowly than macropatch currents, but deactivated at about the same rate.

In contrast, the slowing of current decay for GABA$_A$Rs incorporating the γ1 subunit cannot be attributed to this subunits' contribution to the intrinsic properties of the receptors, as both macropatch and simulated ensemble currents for γ1-containing GABA$_A$Rs had rapid onsets and decays (Figs. 2 and 4). Clearly, then, factors other than the intrinsic kinetic properties of the receptors are responsible for the slower kinetics of the synaptic currents mediated by receptors expressing γ1 subunits. One revealing observation was the reciprocal deactivation pattern for macropatch *versus* synaptic currents between α2β2γ1 and α2β2γ2L GABA$_A$Rs. The deactivation rate for α2β2γ1 receptors was marginally faster than α2β2γ2L receptors in macropatch currents but synaptic currents mediated by α2β2γ1 GABA$_A$Rs were significantly slower than those mediated by α2β2γ2L GABA$_A$Rs, suggesting the γ subunit has a prominent effect on synaptic current kinetics. One possible explanation is that as with the α subunit (37, 38), the γ subunit isoform may also affect receptor clustering at synapses. GABA$_A$Rs that are only loosely clustered at synapses would exhibit slow deactivation kinetics due to slower changes in GABA concentration, whereas GABA$_A$Rs that were more tightly concentrated post-synaptically would give rise to faster current kinetics. Synaptic currents with the slowest kinetics were those generated by α2β2γ1 GABA$_A$Rs, likely because of a combination of the α2 subunit on mean burst duration and the "de-clustering" effect of both α2 and γ1 subunits.

The analysis of αβ receptors in our transfections suggests that, due to their small conductance (~13–14 pS) and infrequent activation (~10% of total), their presence would not make a substantial impact on ensemble currents (macropatch and synaptic) that included the γ subunit. Nevertheless, we also recorded currents in co-cultures transfected only with α1 and

β2 or α2 and β2 subunits to examine if αβ receptors can assemble at synapses. Pure populations of αβ receptors exhibited synaptic currents with rise and decay kinetics that were broadly similar to those of αβγ receptors. α1β2 receptors produced 10–90% rise times of 3.0 ± 0.1 ms and decayed with a mean time constant of 11.0 ± 1.1 ms ($n = 3$). These values were intermediate between those mediated by α1β2γ2L and α1β2γ1 receptors, and an ANOVA test showed no significant difference ($p > 0.05$) between α1β2 receptors and either of their γ-containing counterparts. α2β2 receptors produced mean rise and decay times of 10.5 ± 1.9 and 72.0 ± 15.4 ms, respectively ($n = 4$). As revealed by an ANOVA test, α2β2-mediated synaptic currents were only significantly slower in rise and decay times ($p < 0.05$ for both) to the corresponding measurements of α2β2γ2L-mediated currents. This result is consistent with the γ2L subunit having a clustering effect on receptors, whereas the incorporation of the α2 subunit tended to de-cluster the receptors to produce slower activation rates. The slow decay times in α2β2-mediated currents are also consistent with α2-containing receptors having a higher affinity for GABA. These data demonstrate that αβ receptors can assemble at synaptic sites, as has been demonstrated for α2β3 and α6β3 receptors (38). However, as in our transfections, αβ receptors only constitute about 10% of the overall activity (Fig. 1), their impact on the kinetics of synaptic currents will be minimal.

γ1-Containing GABA$_A$Rs Are Insensitive to Benzodiazepine Current Enhancement—Because γ1-containing receptors have been reported to be less sensitive to benzodiazepine drugs (18, 19, 21), we compared the actions of flunitrazepam and diazepam on IPSCs from cells expressing either α2β2γ1 or α2β2γ2L receptors. As shown in Fig. 6*A*, application of diazepam (1 μM) did not affect α2β2γ1-mediated IPSC decay times (114 ± 7% of control, $n = 4$) but significantly slowed the decay times of currents from α2β2γ2L-expressing cells (171 ± 20% control decay; $p = 0.02$, $n = 4$). Diazepam had no effect on the amplitude of IPSCs (α2β2γ1: 107 ± 13%; α2β2γ2L: 141 ± 15% of control). Flunitrazepam (100 nM) also had no effect on the decay of synaptic currents in α2β2γ1-expressing cells (109 ± 7% of control, $n = 5$) but increased the mean decay time for α2β2γ2L-expressing cells to 212 ± 6% of control ($p < 0.0001$, unpaired *t* test, $n = 4$, Fig. 6). The peak current amplitude trended in a similar way, but was not significantly different between the two receptor types (α2β2γ1, 98 ± 16%; α2β2γ2L, 182 ± 38% of control).

γ-Chimeras Reveal Differential Clustering Properties in Synaptic GABA$_A$Rs—In α subunits, the intracellular domain between TM3 and TM4 has been shown to play a role in clustering GABA$_A$Rs to the synapse via interactions with gephyrin (37, 39). An association between gephyrin and the γ2 subunit was suggested to contribute to synaptic targeting of GABA$_A$Rs (10). Although this has not been confirmed by other studies (14), it remains possible that gephyrin and γ2 interact in mammalian systems, as has been recently shown for the β subunit (13). Interactions with other proteins must mediate gephyrin-independent clustering (5), and the γ subunit could also contribute to these interactions. We tested whether gephyrin and collybistin affected the kinetics of synaptic currents by co-expressing both of these proteins along with either α2β2γ1 or
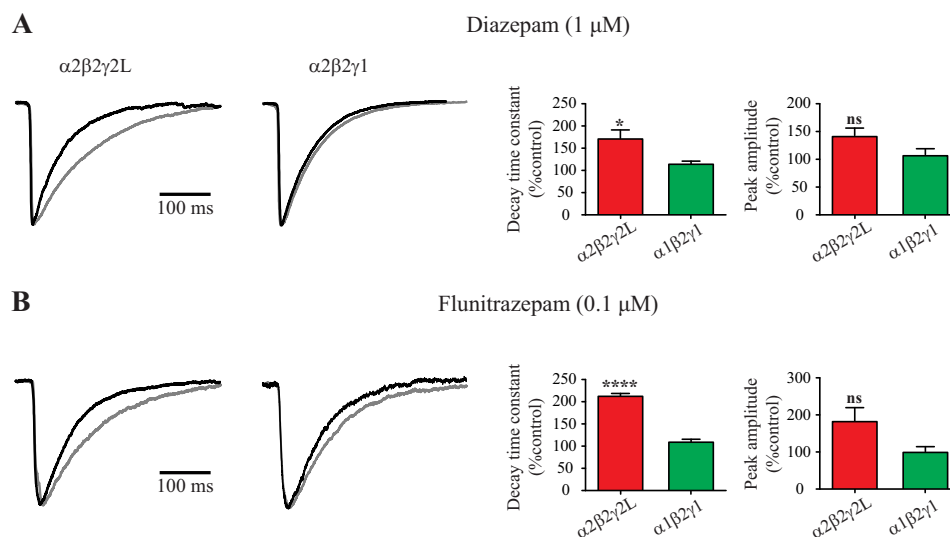
FIGURE 6. **Benzodiazepine pharmacology of γ2L- and γ1-containing GABA$_A$Rs.** Averaged and normalized current traces from multiple cells expressing either α2β2γ2L or α2β2γ1 GABA$_A$Rs before (*black*) and during (*gray*) continuous perfusion of diazepam (*A*) and flunitrazepam (*B*). The accompanying bar plots are pooled data for current decay and peak amplitude. Note that both benzodiazepines markedly slowed the decay rate of α2β2γ2L GABA$_A$Rs (*, $p < 0.05$; ****, $p < 0.0001$), but had no significant (*ns*) effect on α2β2γ1 GABA$_A$Rs. Neither drug significantly altered the peak amplitude of the currents.

α2β2γ2L receptors. The rise and decay times for the α2β2γ1 and α2β2γ2L receptors in combination with these proteins were, respectively, 7.6 $\pm$ 0.6 ($n = 7$) and 4.7 $\pm$ 0.4 ms ($n = 4$) and 52.9 $\pm$ 3.9 and 41.0 $\pm$ 2.2 ms. *t* tests showed that gephyrin and collybistin expression had no significant effect on synaptic current rise times ($p > 0.1$ for both receptors) or decay times ($p > 0.1$; for both receptors). These results demonstrate that gephyrin (and collybistin) have little effect on GABA$_A$R-mediated synaptic currents, as has been suggested by some studies (38, 40). Alternatively, because HEK293 cells endogenously express gephyrin (38), recombinantly expressed gephyrin may have no additional effect on current kinetics.

The IDs of the γ1 and γ2L show considerable sequence divergence and their TM4 domains vary at sites that correspond to those shown to be essential for γ2-mediated receptor clustering in cultured neurons (12). Given these observations, we tested the possibility that the γ subunit isoform was also affecting synaptic clustering, by making chimeras of the γ1 and γ2L subunits that replace the ID and TM4 of one isoform with that of the other. This produced two γ-chimeric subunits, γ2L-γ1 and γ1-γ2L (Fig. 7A), which were then cotransfected with α2 and β2 subunits. These transfections also produced robust spontaneous synaptic activity, of comparable frequency and amplitude to the wild-type receptors. Synaptic currents mediated by the α2β2γ1-γ2L GABA$_A$Rs activated with a mean 10–90% rise time of 4.4 $\pm$ 0.5 ms ($n = 5$) and deactivated with a mean weighted time constant of 38.2 $\pm$ 2.4 ms (Fig. 7B). This current profile was indistinguishable from that of the wild-type α2β2γ2L receptors (Fig. 7C). Similarly, the α2β2γ2L-γ1 receptors exhibited activation and deactivation rates of 7.4 $\pm$ 1.1 and 53.5 $\pm$ 7.2 ms ($n = 5$), respectively, and these too were similar to wild-type α2β2γ1 GABA$_A$Rs (Fig. 7, *B* and *C*). A two-way ANOVA confirmed that the ID plus the TM4 region had a significant effect on activation and deactivation rates ($p < 0.001$ for both), whereas the extracellular domain and TM1–3 did not ($p > 0.1$ for both). These observations show that the γ subunit
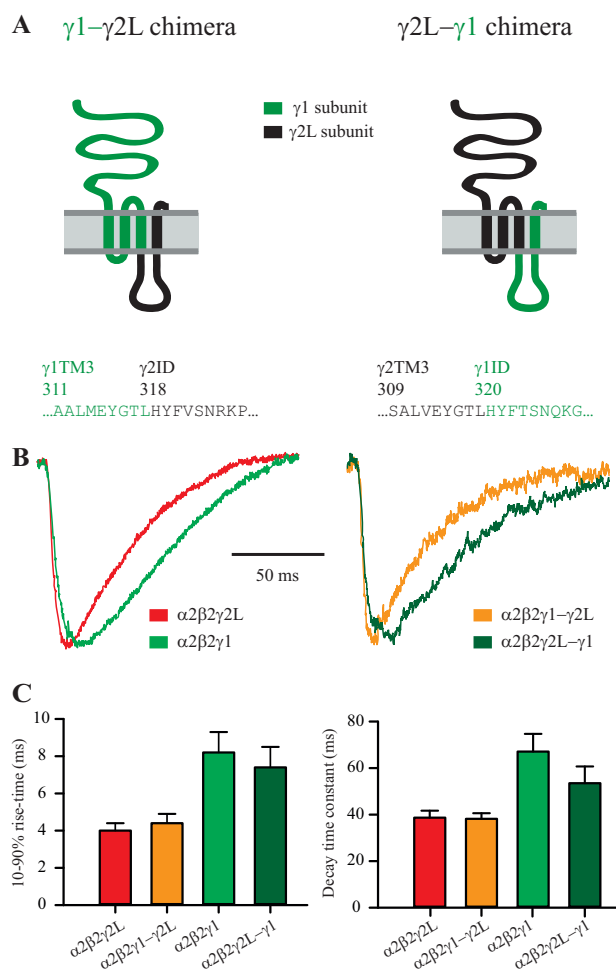
isoform is a major contributor to the kinetic profile of synaptic currents and the ID and TM4 likely mediates this effect.

DISCUSSION

In this study we have shown that the presence of the α2 subunit slows the deactivation phase of the IPSC by increasing the receptors' affinity for GABA, whereas inclusion of the α2 and γ1 subunits slows both the activation and deactivation phases of the IPSC by conferring loose clustering properties to the receptors. The presence of the γ1 subunit results in IPSCs with markedly slower activation and deactivation phases, and the kinetics of chimeras of γ1 and γ2 subunits are in agreement with this proposal. Together, these data suggest that GABA$_A$Rs containing γ1 and γ2 subunits use different mechanisms for synaptic clustering.

We first determined the kinetic properties of four subtypes of GABA$_A$Rs that vary in their α (α1 or α2) and/or γ (γ1 or γ2L) subunit isoform, whereas keeping the β subunit constant. Brief ($<$1 ms) GABA application onto macropatches elicited currents that mimic those at synapses, but are unaffected by factors that are not related to the inherent properties of the receptors. The receptor kinetic properties were further investigated on a single channel level, and within the framework of a single activation mechanism, facilitating a correlation between subunit isoform, GABA affinity, and the efficacy with which GABA activated the receptors (41). Macropatch currents mediated by all four GABA$_A$Rs activated with sub-millisecond rates, with α2-containing receptors activating marginally more slowly. The inclusion of the α2 subunit also slowed current deactivation by almost an order of magnitude.

An analysis of the discrete activations (clusters and bursts) showed that the durations of these activations was α subunit dependent. At a low GABA concentration, α1-containing receptors activated for mean durations of 23–27 ms, whereas the presence of α2 subunits lengthened the bursts to 60–100 ms. Single channel data were also used to derive an activation

A

γ1–γ2L chimera   **γ2L–γ1 chimera**

- ■ γ1 subunit
- ■ γ2L subunit

γ1TM3	γ2ID		γ2TM3	γ1ID
311	318		309	320
...AALMEYGTLHYFVSNRKP...			...SALVEYGTLHYFTSNQKG...	

B

50 ms

α2β2γ2L
α2β2γ1

α2β2γ1–γ2L
α2β2γ2L–γ1

C

FIGURE 7. **γ1 subunits slow synaptic current kinetics.** *A*, schematic representation of the subunit chimeras used to investigate γ subunit related synaptic clustering. Swapping the intracellular and TM4 domains made the chimeras. *B*, averaged synaptic currents recorded from heterosynapses expressing the wild-type α2β2γ2L and α2β2γ1 (reproduced from Fig. 5) and chimeric α2β2γ1-γ2L and α2β2γ1-γ2L GABA$_A$Rs. Note the similar activation and deactivation between wild-type and corresponding chimeric GABA$_A$Rs. *C*, averaged values for activation and deactivation for the wild-type and chimeric GABA$_A$Rs showing that both activation and deactivation are strongly dependent on the ID plus TM4 domains of the γ subunit.

mechanism that accurately described the single channel and macropatch data of all four GABA$_A$Rs. This scheme comprised two sequential, equivalent binding steps for GABA followed by three shut and three open functional states (Fig. 4*B*). Given similar models have previously been applied to other isoforms of GABA$_A$Rs (7, 25), our activation scheme may be generally applicable to other synaptic GABA$_A$R stoichiometries. This consensus mechanism suggests that the essential contribution made by the α2 subunit is to enhance the GABA binding affinity 3–4-fold, thereby increasing the durations of bursts. A similar result was observed for α3-containing GABA$_A$Rs (7). The discrepancy in ligand affinity between α1- and α2-containing GABA$_A$Rs is compatible with the significant primary sequence divergence at the GABA binding domains of these two subunits. A common feature of all schemes that were tested here, and indeed for mechanisms derived for other pentameric ligand-gated ion channels (42–46) is the presence of at least one shut-to-shut state transition immediately following the

binding reaction steps. The equilibrium constant describing the transition between these two shut states was denoted as Φ and it is intriguing that macropatch and single channel analysis failed to detect any kinetic parameter that could be attributed to the γ subunit isoform other than Φ. This constant was <1 only if the receptor expressed the γ1 isoform and may pertain to GABA$_A$R modulation by benzodiazepines, which a recent study has shown to manifest as an enhancement of Φ in γ2-containing GABA$_A$Rs (47). Our data are consistent with the notion that Φ is γ isoform dependent, the lower value of Φ for γ1-containing receptors might suggest a reduced capacity for enhancement by benzodiazepine modulators.

Transfecting HEK293 cells with GABA$_A$R subunits together with neuroligin 2A, and co-culturing these on a bed of neurons induces the formation of functional synapses between neurons and HEK293 cells (48), demonstrating that all of the essential pre- and post-synaptic elements are present in the artificial system, including neurexin, which is endogenously expressed in neurons, and gephyrin, which is present in HEK293 cells (38).

At these synapses notable pharmacological differences were observed between γ1-containing and γ2L-containing GABA$_A$Rs. Experiments using flunitrazepam and diazepam demonstrate that benzodiazepines are ineffective at enhancing synaptic currents mediated by γ1-containing GABA$_A$Rs. This result is consistent with whole cell peak current measurements of γ1-containing GABA$_A$Rs (18), and key differences in the amino acid sequence between γ2L and γ1 that have been shown to affect the potency with which benzodiazepine-site ligands modulate currents (49–52).

In addition, our results show that the α2 and γ1 subunits have de-clustering effects when expressed at synapses. Using chimeric constructs we show that the ID (plus TM4) is responsible for this difference in the γ-subunit. The ID and TM4 of GABA receptor subunits is crucial for clustering of receptors at post-synaptic sites (12), and our results suggest that, at these engineered synapses, γ1- and γ2L-containing GABA$_A$Rs have different synaptic kinetics because of differences in their clustering properties. Thus, at neuronal synapses *in situ*, it is possible that GABA receptors containing γ1 and γ2 subunits may also be differentially targeted (18, 53). Subunit-specific clustering mechanisms have already been noted for α subunits in neurons. For example, dystrophin is currently thought to be involved in anchoring dendritic clusters of α1 in specific cortical layers (15), and radaxin has been shown to selectively anchor α5 subunits (54). Differential clustering properties have also been demonstrated for α1 and α2 subunits, such as the lower affinity of the α2 subunit for gephyrin (37) and the recruitment of α2, but not α1 subunits to the axon initial segment (55).

Postsynaptic GABA$_A$Rs are dynamic, diffusing in and out of the synaptic active zone, which is ~200–300 nm in diameter (56, 57), with a diffusion coefficient that ranges from 0.01 to 0.05 $\mu m^2 \, s^{-1}$ (56). Quantum dot and Immunogold-labeled GABA$_A$Rs show sub-micrometer separations between GABA$_A$Rs that appose the presynaptic density and those that are perisynaptic (57, 58), whereas extrasynaptic GABA$_A$Rs, such as those containing the δ subunit, are generally located hundreds of nanometers to several micrometers further (38, 57). These observations are consistent with a concentration gradient of receptors that is an

inverse function of receptor diffusion mobility. We interpret our data as being consistent with a differential, γ-isoform-dependent gradient of receptors, rather than mutually exclusive zones delineating synaptic receptors from those beyond the synaptic perimeter. The slower rise and decay times for γ1-containing GABA$_A$Rs suggest that these receptors are more mobile and at a higher density outside the synapse than γ2L-containing receptors, whereas the converse would apply for γ2L-containing receptors. Within this context we refer to γ2L-containing GABA$_A$Rs as being more tightly clustered at synapses where a higher proportion are perfused with high GABA prior to significant GABA diffusion.

Our findings evince key factors that determine the profile of synaptic currents mediated by GABA$_A$Rs containing α1, α2, γ1, and γ2L subunits, and provide a solid basis for future studies to establish whether GABA$_A$Rs containing α2 and γ1 subunits contribute to GABAergic synapses in key brain regions that mediate fear and anxiety (59).

REFERENCES

1. Olsen, R. W., and Sieghart, W. (2008) International Union of Pharmacology. LXX. Subtypes of γ-aminobutyric acid(A) receptors. Classification on the basis of subunit composition, pharmacology, and function. Update. *Pharmacol. Rev.* **60,** 243–260

2. Pirker, S., Schwarzer, C., Wieselthaler, A., Sieghart, W., and Sperk, G. (2000) GABA(A) receptors. Immunocytochemical distribution of 13 subunits in the adult rat brain. *Neuroscience* **101,** 815–850

3. Schofield, C. M., and Huguenard, J. R. (2007) GABA affinity shapes IPSCs in thalamic nuclei. *J. Neurosci.* **27,** 7954–7962

4. Eyre, M. D., Renzi, M., Farrant, M., and Nusser, Z. (2012) Setting the time course of inhibitory synaptic currents by mixing multiple GABA(A) receptor α subunit isoforms. *J. Neurosci.* **32,** 5853–5867

5. Kneussel, M., Brandstätter, J. H., Gasnier, B., Feng, G., Sanes, J. R., and Betz, H. (2001) Gephyrin-independent clustering of postsynaptic GABA(A) receptor subtypes. *Mol. Cell. Neurosci.* **17,** 973–982

6. Körber, C., Richter, A., Kaiser, M., Schlicksupp, A., Mükusch, S., Kuner, T., Kirsch, J., and Kuhse, J. (2012) Effects of distinct collybistin isoforms on the formation of GABAergic synapses in hippocampal neurons. *Mol. Cell. Neurosci.* **50,** 250–259

7. Keramidas, A., and Harrison, N. L. (2010) The activation mechanism of α1β2γ2S and α3β3γ2S GABAA receptors. *J. Gen. Physiol.* **135,** 59–75

8. Lavoie, A. M., Tingey, J. J., Harrison, N. L., Pritchett, D. B., and Twyman, R. E. (1997) Activation and deactivation rates of recombinant GABA(A) receptor channels are dependent on α-subunit isoform. *Biophys. J.* **73,** 2518–2526

9. Okada, M., Onodera, K., Van Renterghem, C., Sieghart, W., and Takahashi, T. (2000) Functional correlation of GABA(A) receptor α subunits expression with the properties of IPSCs in the developing thalamus. *J. Neurosci.* **20,** 2202–2208

10. Essrich, C., Lorez, M., Benson, J. A., Fritschy, J. M., and Lüscher, B. (1998) Postsynaptic clustering of major GABAA receptor subtypes requires the γ2 subunit and gephyrin. *Nat. Neurosci.* **1,** 563–571

11. Fritschy, J. M., Harvey, R. J., and Schwarz, G. (2008) Gephyrin. Where do we stand, where do we go? *Trends Neurosci.* **31,** 257–264

12. Alldred, M. J., Mulder-Rosi, J., Lingenfelter, S. E., Chen, G., and Lüscher, B. (2005) Distinct γ2 subunit domains mediate clustering and synaptic function of postsynaptic GABAA receptors and gephyrin. *J. Neurosci.* **25,** 594–603

13. Kowalczyk, S., Winkelmann, A., Smolinsky, B., Förstera, B., Neundorf, I.,

14. Schwarz, G., and Meier, J. C. (2013) Direct binding of GABAA receptor β2 and β3 subunits to gephyrin. *Eur. J. Neurosci.* **37,** 544–554

15. Saiepour, L., Fuchs, C., Patrizi, A., Sassoè-Pognetto, M., Harvey, R. J., and Harvey, K. (2010) Complex role of collybistin and gephyrin in GABAA receptor clustering. *J. Biol. Chem.* **285,** 29623–29631

16. Panzanelli, P., Gunn, B. G., Schlatter, M. C., Benke, D., Tyagarajan, S. K., Scheiffele, P., Belelli, D., Lambert, J. J., Rudolph, U., and Fritschy, J. M. (2011) Distinct mechanisms regulate GABAA receptor and gephyrin clustering at perisomatic and axo-axonic synapses on CA1 pyramidal cells. *J. Physiol.* **589,** 4959–4980

17. Günther, U., Benson, J., Benke, D., Fritschy, J. M., Reyes, G., Knoflach, F., Crestani, F., Aguzzi, A., Arigoni, M., and Lang, Y. (1995) Benzodiazepine-insensitive mice generated by targeted disruption of the γ2 subunit gene of γ-aminobutyric acid type A receptors. *Proc. Natl. Acad. Sci. U.S.A.* **92,** 7749–7753

18. Esmaeili, A., Lynch, J. W., and Sah, P. (2009) GABA$_A$ receptors containing γ1 subunits contribute to inhibitory transmission in the central amygdala. *J. Neurophysiol.* **101,** 341–349

19. Ymer, S., Draguhn, A., Wisden, W., Werner, P., Keinänen, K., Schofield, P. R., Sprengel, R., Pritchett, D. B., and Seeburg, P. H. (1990) Structural and functional characterization of the γ1 subunit of GABA$_A$/benzodiazepine receptors. *EMBO J.* **9,** 3261–3267

20. Nusser, Z., Cull-Candy, S., and Farrant, M. (1997) Differences in synaptic GABA(A) receptor number underlie variation in GABA mini amplitude. *Neuron* **19,** 697–709

21. Wafford, K. A., Whiting, P. J., and Kemp, J. A. (1993) Differences in affinity and efficacy of benzodiazepine receptor ligands at recombinant γ-aminobutyric acidA receptor subtypes. *Mol. Pharmacol.* **43,** 240–244

22. Chih, B., Gollan, L., and Scheiffele, P. (2006) Alternative splicing controls selective trans-synaptic interactions of the neuroligin-neurexin complex. *Neuron* **51,** 171–178

23. Brewer, G. J. (1995) Serum-free B27/neurobasal medium supports differentiated growth of neurons from the striatum, substantia nigra, septum, cerebral cortex, cerebellum, and dentate gyrus. *J. Neurosci. Res.* **42,** 674–683

24. Barry, P. H. (1994) JPCalc, a software package for calculating liquid junction potential corrections in patch-clamp, intracellular, epithelial and bilayer measurements and for correcting junction potential measurements. *J. Neurosci. Methods* **51,** 107–116

25. Lema, G. M., and Auerbach, A. (2006) Modes and models of GABA(A) receptor gating. *J. Physiol.* **572,** 183–200

26. Colquhoun, D., and Sigworth, F. J. (1995) *Fitting and statistical analysis of single-channel records.* In *Single-Channel Recordings*, 2 Ed., pp. 483–585, Plenum Press, New York

27. Qin, F., Auerbach, A., and Sachs, F. (1997) Maximum likelihood estimation of aggregated Markov processes. *Proc. Biol. Sci.* **264,** 375–383

28. Angelotti, T. P., and Macdonald, R. L. (1993) Assembly of GABAA receptor subunits. α1β1 and α1β1γ 2S subunits produce unique ion channels with dissimilar single-channel properties. *J. Neurosci.* **13,** 1429–1440

29. Lorez, M., Benke, D., Luscher, B., Mohler, H., and Benson, J. A. (2000) Single-channel properties of neuronal GABA$_A$ receptors from mice lacking the 2 subunit. *J. Physiol.* **527,** 11–31

30. Keramidas, A., and Harrison, N. L. (2008) Agonist-dependent single channel current and gating in α4β2δ and α1β2γ2S GABA$_A$ receptors. *J. Gen. Physiol.* **131,** 163–181

31. Keramidas, A., Kash, T. L., and Harrison, N. L. (2006) The pre-M1 segment of the α1 subunit is a transduction element in the activation of the GABA$_A$ receptor. *J. Physiol.* **575,** 11–22

32. McClellan, A. M., and Twyman, R. E. (1999) Receptor system response kinetics reveal functional subtypes of native murine and recombinant human GABA$_A$ receptors. *J. Physiol.* **515,** 711–727

33. Wyllie, D. J., Behe, P., and Colquhoun, D. (1998) Single-channel activations and concentration jumps. Comparison of recombinant NR1a/NR2A and NR1a/NR2D NMDA receptors. *J. Physiol.* **510,** 1–18

34. Elenes, S., Ni, Y., Cymes, G. D., and Grosman, C. (2006) Desensitization contributes to the synaptic response of gain-of-function mutants of the

muscle nicotinic receptor. *J. Gen. Physiol.* **128,** 615–627

35. Sine, S. M., and Engel, A. G. (2006) Recent advances in Cys-loop receptor structure and function. *Nature* **440,** 448–455

36. Jones, M. V., and Westbrook, G. L. (1995) Desensitized states prolong GABAA channel responses to brief agonist pulses. *Neuron* **15,** 181–191

37. Maric, H. M., Mukherjee, J., Tretter, V., Moss, S. J., and Schindelin, H. (2011) Gephyrin-mediated γ-aminobutyric acid type A and glycine receptor clustering relies on a common binding site. *J. Biol. Chem.* **286,** 42105–42114

38. Wu, X., Wu, Z., Ning, G., Guo, Y., Ali, R., Macdonald, R. L., De Blas, A. L., Luscher, B., and Chen, G. (2012) γ-Aminobutyric acid type A (GABAA) receptor α subunits play a direct role in synaptic versus extrasynaptic targeting. *J. Biol. Chem.* **287,** 27417–27430

39. Tretter, V., Jacob, T. C., Mukherjee, J., Fritschy, J. M., Pangalos, M. N., and Moss, S. J. (2008) The clustering of GABA(A) receptor subtypes at inhibitory synapses is facilitated via the direct binding of receptor α2 subunits to gephyrin. *J. Neurosci.* **28,** 1356–1365

40. Lévi, S., Logan, S. M., Tovar, K. R., and Craig, A. M. (2004) Gephyrin is critical for glycine receptor clustering but not for the formation of functional GABAergic synapses in hippocampal neurons. *J. Neurosci.* **24,** 207–217

41. Colquhoun, D. (1998) Binding, gating, affinity and efficacy. The interpretation of structure-activity relationships for agonists and of the effects of mutating receptors. *Br. J. Pharmacol.* **125,** 924–947

42. Lape, R., Colquhoun, D., and Sivilotti, L. G. (2008) On the nature of partial agonism in the nicotinic receptor superfamily. *Nature* **454,** 722–727

43. Mukhtasimova, N., Lee, W. Y., Wang, H. L., and Sine, S. M. (2009) Detection and trapping of intermediate states priming nicotinic receptor channel opening. *Nature* **459,** 451–454

44. Jadey, S., and Auerbach, A. (2012) An integrated catch-and-hold mechanism activates nicotinic acetylcholine receptors. *J. Gen. Physiol.* **140,** 17–28

45. Krashia, P., Lape, R., Lodesani, F., Colquhoun, D., and Sivilotti, L. G. (2011) The long activations of α2 glycine channels can be described by a mechanism with reaction intermediates ("flip"). *J. Gen. Physiol.* **137,** 197–216

46. Lape, R., Plested, A. J., Moroni, M., Colquhoun, D., and Sivilotti, L. G. (2012) The α1K276E startle disease mutation reveals multiple intermediate states in the gating of glycine receptors. *J. Neurosci.* **32,** 1336–1352

47. Gielen, M. C., Lumb, M. J., and Smart, T. G. (2012) Benzodiazepines modulate GABA_A receptors by regulating the preactivation step after GABA binding. *J. Neurosci.* **32,** 5707–5715

48. Dong, N., Qi, J., and Chen, G. (2007) Molecular reconstitution of functional GABAergic synapses with expression of neuroligin-2 and GABA_A receptors. *Mol. Cell. Neurosci.* **35,** 14–23

49. Wingrove, P. B., Thompson, S. A., Wafford, K. A., and Whiting, P. J. (1997) Key amino acids in the γ subunit of the γ-aminobutyric acid A receptor that determine ligand binding and modulation at the benzodiazepine site. *Mol. Pharmacol.* **52,** 874–881

50. Buhr, A., and Sigel, E. (1997) A point mutation in the γ2 subunit of γ-aminobutyric acid type A receptors results in altered benzodiazepine binding site specificity. *Proc. Natl. Acad. Sci. U.S.A.* **94,** 8824–8829

51. Buhr, A., Baur, R., and Sigel, E. (1997) Subtle changes in residue 77 of the γ subunit of α1β2γ2 GABA_A receptors drastically alter the affinity for ligands of the benzodiazepine binding site. *J. Biol. Chem.* **272,** 11799–11804

52. Hanson, S. M., and Czajkowski, C. (2008) Structural mechanisms underlying benzodiazepine modulation of the GABA(A) receptor. *J. Neurosci.* **28,** 3490–3499

53. Delaney, A. J., and Sah, P. (2001) Pathway-specific targeting of GABA(A) receptor subtypes to somatic and dendritic synapses in the central amygdala. *J. Neurophysiol.* **86,** 717–723

54. Loebrich, S., Bähring, R., Katsuno, T., Tsukita, S., and Kneussel, M. (2006) Activated radixin is essential for GABA(A) receptor α5 subunit anchoring at the actin cytoskeleton. *EMBO J.* **25,** 987–999

55. Thomson, A. M., and Jovanovic, J. N. (2010) Mechanisms underlying synapse-specific clustering of GABA(A) receptors. *Eur. J. Neurosci.* **31,** 2193–2203

56. Ribrault, C., Sekimoto, K., and Triller, A. (2011) From the stochasticity of molecular processes to the variability of synaptic transmission. *Nat. Rev. Neurosci.* **12,** 375–387

57. Nusser, Z., Sieghart, W., and Somogyi, P. (1998) Segregation of different GABA_A receptors to synaptic and extrasynaptic membranes of cerebellar granule cells. *J. Neurosci.* **18,** 1693–1703

58. Bannai, H., Lévi, S., Schweizer, C., Inoue, T., Launey, T., Racine, V., Sibarita, J. B., Mikoshiba, K., and Triller, A. (2009) Activity-dependent tuning of inhibitory neurotransmission based on GABA_AR diffusion dynamics. *Neuron* **62,** 670–682

59. Crestani, F., Lorez, M., Baer, K., Essrich, C., Benke, D., Laurent, J. P., Belzung, C., Fritschy, J. M., Lüscher, B., and Mohler, H. (1999) Decreased GABA_A-receptor clustering results in enhanced anxiety and a bias for threat cues. *Nat. Neurosci.* **2,** 833–839